NSRRC-J04751 (2015)

Colloids and Surfaces B: Biointerfaces 128 (2015) 67–76

Contents lists available at ScienceDirect

Colloids and Surfaces B: Biointerfaces

journal homepage: www.elsevier.com/locate/colsurfb

Development of a diagnostic polymersome system for potential imaging delivery

Wen-Chia Huang[a], Yung-Chu Chen[b], Yuan-Hung Hsu[b], Wen-Yuan Hsieh[b,*], Hsin-Cheng Chiu[a,*]

[a] Department of Biomedical Engineering and Environmental Sciences, National Tsing Hua University, Hsinchu 300, Taiwan
[b] Biomedical Technology and Device Research Laboratory, Industrial Technology Research Institute, Hsinchu 300, Taiwan

ARTICLE INFO

Article history:
Received 17 October 2014
Received in revised form 30 January 2015
Accepted 4 February 2015
Available online 14 February 2015

Keywords:
Diagnostic polymersomes
Magnetic resonance imaging (MRI)
Near-infrared (NIR) imaging
Cancer diagnosis

ABSTRACT

In order to enhance visualization of soft tissues, a dual-imaging diagnostic polymersome system featured with highly hydrated multilamellar wall structure capable of simultaneously embedding a hydrophobic near-infrared fluorophore, Cy5.5, and a paramagnetic probe, gadolinium (Gd(III)) cations was developed. The polymersomes were obtained from the self-assembly of lipid-containing copolymer, poly(acrylic acid-co-distearin acrylate), in aqueous solution. The Cy5.5 and Gd(III) species were loaded into polymersomes *via* hydrophobic association (loading efficiency of Cy5.5 *ca* 74%) and electrostatic complexation (Gd(III) 83%), respectively. The Cy5.5/Gd(III)-loaded polymersomes (CGLPs) have shown excellent payload confinement, reduced dilution effect on assembly dissociation and decreased protein/salt-induced colloidal aggregation. Owing to the highly hydrated structure of vesicular membrane, the superior contrast enhancement of CGLPs in magnetic resonance (MR) imaging was obtained as a result of prolonged rotational correlation time of Gd(III) cations and fast water exchange from Gd(III) to bulk solution. The CGLPs exhibit a 15-fold higher longitudinal relaxivity value (*ca* 60 mM^{-1} s^{-1}) than that (4 mM^{-1} s^{-1}) of the commercial contrast agent, Magnevist, in phosphate buffered saline. The *in vivo* characterization demonstrates that CGLPs exhibit a signal-to-noise ratio in T_1-weighted MR image contrast similar to that of Magnevist, yet with a Gd dose 5-fold lower. An excellent contrast in NIR imaging at tumor site was attained following the intravenous injection of GGLPs into Tramp-C1 tumor-bearing mice (C57BL/6). Along with their non-toxicity at the dose used, these results demonstrate the great potential of the CGLPs as an advanced diagnostic nanodevice.

© 2015 Elsevier B.V. All rights reserved.

1. Introduction

For improving cancer therapy efficacy, imaging contrast agents are usually required to assist evaluating disease states and highlight differences between normal and abnormal tissues prior to the therapy process [1–4]. Along with the advance in medical imaging technology, a variety of noninvasive imaging modalities have been utilized to facilitate the early detection of cancer [5]. Magnetic resonance (MR) imaging is one of the powerful and non-invasive imaging techniques to obtain high resolution, three-dimensional body images [6–8]. However, small gadolinium (Gd) ion complexes serving as T_1-weighted contrast agents in clinical MRI diagnosis frequently suffer from rapid renal clearance, non-specific tissue accumulation, and low contrast efficiency. The use of supramolecular Gd(III) complexes in MR imaging applications has shown many practical advantages, such as high contrast in blood-pool imaging [9] and long blood circulation half-life [10], over that using small Gd(III) complexes [11]. Another popular imaging technique is optical imaging that is often utilized for accurately detecting the accumulation of nanoparticulate delivery systems at target sites by using a near-infrared (NIR) fluorophore with emission wavelengths larger than 620 nm where the auto-fluorescence is minimized [12]. Nevertheless, there are still several limitations in every modality such as low sensitivity, low spatial resolution and inaccurate diagnosis due to undesired accumulation of diagnostic agents to non-target organs [13]. Multi-modal imaging delivery systems bearing each individual benefits may be advantageous in overcoming the limitations associated with the stand-alone systems [14].

To develop a multi-modal imaging delivery system, polymer assemblies are attractive due to their unique assembly

* Corresponding authors.
E-mail addresses: hsiehw@itri.org.tw (W.-Y. Hsieh), hscchiu@mx.nthu.edu.tw (H.-C. Chiu).

http://dx.doi.org/10.1016/j.colsurfb.2015.02.008
0927-7765/© 2015 Elsevier B.V. All rights reserved.

architectures wherein the hydrophobic domains can serve as a depot for hydrophobic cargos while ionic payloads can be entrapped within oppositely charged polyelectrolyte outer layer by electrostatic complexation. The polymer assemblies can thus readily act as a supramolecular contrast agent by pertinent loading with paramagnetic components or optical luminescent probes within assembly structures. In our previous works [15–18], the pH-responsive polymersomes obtained from spontaneous assembly of the lipid-containing copolymers, poly(acrylic acid-co-distearin acrylate) (poly(AAc-co-DSA)) have shown the capability of loading cationic species into polymeric vesicle membrane *via* charge interaction with ionized AAc residues. With a high negative charge density within polymer multilemellar walls, hydrophilic cationic species can preferentially penetrate into the interior structure of vesicle membrane and subsequently attach onto hydrated vesicular multilayers by virtue of ionic complexation with ionized AAc residues.

Herein, we propose a novel dual-imaging diagnostic polymersome system in which excellent NIR/MR imaging contrasts are attained by NIR fluorescence-emitting Cy5.5 and paramagnetic Gd(III) species. The hydrated multilamellar structure renders the Cy5.5/Gd(III)-loaded polymersomes (CGLPs) from poly(AAc-co-DSA) capable of firmly confining diagnostic payloads by hydrophobic interactions of close-packed lipid bilayer islets with Cy5.5 and electrostatic association of ionized AA residues within hydrated interlayer with Gd(III) (Fig. 1). The multilamellar assembly architecture of CGLPs also exhibits several characteristics pertinent to enhanced colloidal stability against large volume dilution and protein/salt-induced aggregation, prolonged rotational correlation time of the embedded Gd(III) cations, and promoted water exchange from Gd(III) to bulk solution.

2. Materials and methods

2.1. Materials

Synthesis and characterization of the poly(AAc-co-DSA) copolymer are described in detail in Supplementary Data (SD). $GdCl_3$ was obtained from Aldrich–Sigma. Human cervical tumor cell line (HeLa cell) was purchased from the Food Industry Research and Development Institute of Taiwan. The Dulbecco's modified Eagle medium (DMEM) was purchased from Invitrogen. AlamarBlue was purchased from AbD Serotec. Deionized water was produced by the Milli-Q Synthesis System (18 MΩ, Millipore). All chemicals are reagent grade and used as received.

2.2. Preparation of CGLPs

Poly(AAc-co-DSA) (10.0 mg) and Cy5.5 (400 μg) were dissolved in 1 mL THF. The Cy5.5/copolymer solution (0.1 mL) was added dropwise into acetate buffer (pH 5.0, 3.0 mL, ionic strength 0.01 M). The mixture was subjected to ultrasonication at 25 °C for 10 min. After repeated ultrafiltration (Amicon 8010 with a Millipore PBMK membrane, MWCO 100k) with pH 5.0 acetate buffer to remove THF, the polymer solution was concentrated to a final concentration of *ca* 1.67 mg/mL. The Cy5.5-loaded polymersomes were thus attained. The aqueous solution of $GdCl_3$ (0.01 M, 62 μL) was added directly into the polymersome suspension (pH 7.4, 2.0 mL) to a final concentration of 2×10^{-4} M. The suspension was then stirred at 4 °C for 12 h to complete the Gd(III) loading process. To eliminate the unbound Gd(III) species, the CGLP suspension was further dialyzed (Cellu Sep MWCO 12,000–14,000) against pH 5.0 buffer for 3 days. The loading quantification is described in SD.

2.3. Laser light scattering measurements

In this study, the ratio of the gyration and hydrodynamic radii (R_g/R_h) of the polymer assemblies was used to assess the assembly morphology as a function of pH. The medium pH was adjusted by either NaOH or HCl aqueous solution. The mean hydrodynamic radius (R_h) was attained by dynamic light scattering (DLS) on a Brookhaven BI-200SM goniometer equipped with a BI-9000 AT digital correlator using a solid-state laser (30 mW, $\lambda = 637$ nm) at 90°. The CONTIN algorithm method was employed to confirm the absence of bimodal particle size distribution of polymeric assemblies with much enhanced reliability [16,19]. The weight-average molar mass (M_w) and R_g of polymeric assemblies were evaluated by static light scattering from the Berry treatment of the angular dependent measurements of the time-averaged intensity of scattered light for a series of concentrations of polymeric assemblies (75–120 μg/mL) in aqueous suspensions [20,21]. The d*n*/d*c* values of the aqueous phases as the media to disperse polymer assemblies were obtained by a BI-DNDC differential refractometer ($\lambda = 620$ nm).

2.4. SAXS measurements

For the SAXS experiments, samples were run at beamline 23A1 at the National Synchrotron Radiation Research Center, Hsinchu, Taiwan. The energy of X-ray source was 14 keV. A small amount of the polymersome suspension (10.0 mg/mL) at the preset pH was placed in the center of a steel washer and closely sealed with Kapton tape and run for 5 min. The scattering signals were collected by MarCCD detector with a pixel resolution of 512 × 512. The scattering intensity profile was depicted from the scattering intensity, $I(q)$, versus the scattering vector, $q = (4\pi/\lambda)\sin(\theta/2)$ (where θ is the scattering angle), after corrections for solvent background, sample transmission, empty cell transmission, empty cell scattering and the detector sensitivity [15].

2.5. The longitudinal relaxation time (T_1) measurements of CGLPs

The relaxation parameter (T_1) was determined by a relaxometer (Bruker Minispec mq20) at 37 °C. The inversion recovery method was adopted in order to obtain longitudinal relaxivity (r_1) from Eq. (1) shown below. The observed relaxation rate $(1/T_1)_{obs}$ of water protons is comprised of both diamagnetic and paramagnetic contributions. The paramagnetic contribution is linearly related to the concentration of paramagnetic species, in this event the Gd(III) cations present in the system [2,22].

$$\left(\frac{1}{T_1}\right)_{obs} = \left(\frac{1}{T_1}\right)_{dia} + r_1[\mathrm{Gd}] \quad (1)$$

The measurements were performed with CGLP suspensions in the pH 7.4 buffer and in phosphate buffered saline (PBS), respectively. The Gd(III) concentration in the CGLP suspension was determined by ICP-MS prior to longitudinal relaxation time measurements.

2.6. Cellular uptake and cytotoxicity

HeLa cells were cultured in DMEM with 1.0% penicillin–streptomycin (Pen–Strep) and 10% fetal bovine serum (FBS) in a humidified incubator at 37 °C and 5% CO_2 for 2 days. Cells were harvested by addition of a 0.25% (w/v) trypsin–0.03% (w/v) EDTA solution, re-suspended in DMEM, and placed in a 96-well plate (8000 cells/well) for 24 h prior to the cytotoxicity analysis. The culture medium was replaced with DMEM (10% FBS, 1% Pen–Strep) containing $GdCl_3$ or CGLPs at equivalent Gd(III) concentrations for 24 h at 37 °C. The medium was removed and

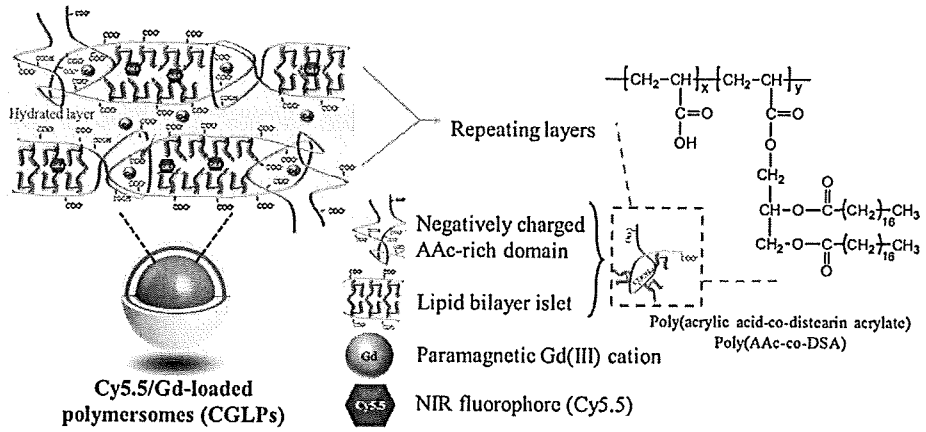

Fig. 1. Schematic illustration of the diagnostic polymersomes capable of simultaneously embedding the hydrophobic NIR fluorophore, Cy5.5, and the paramagnetic probe, Gd(III), within vesicular walls.

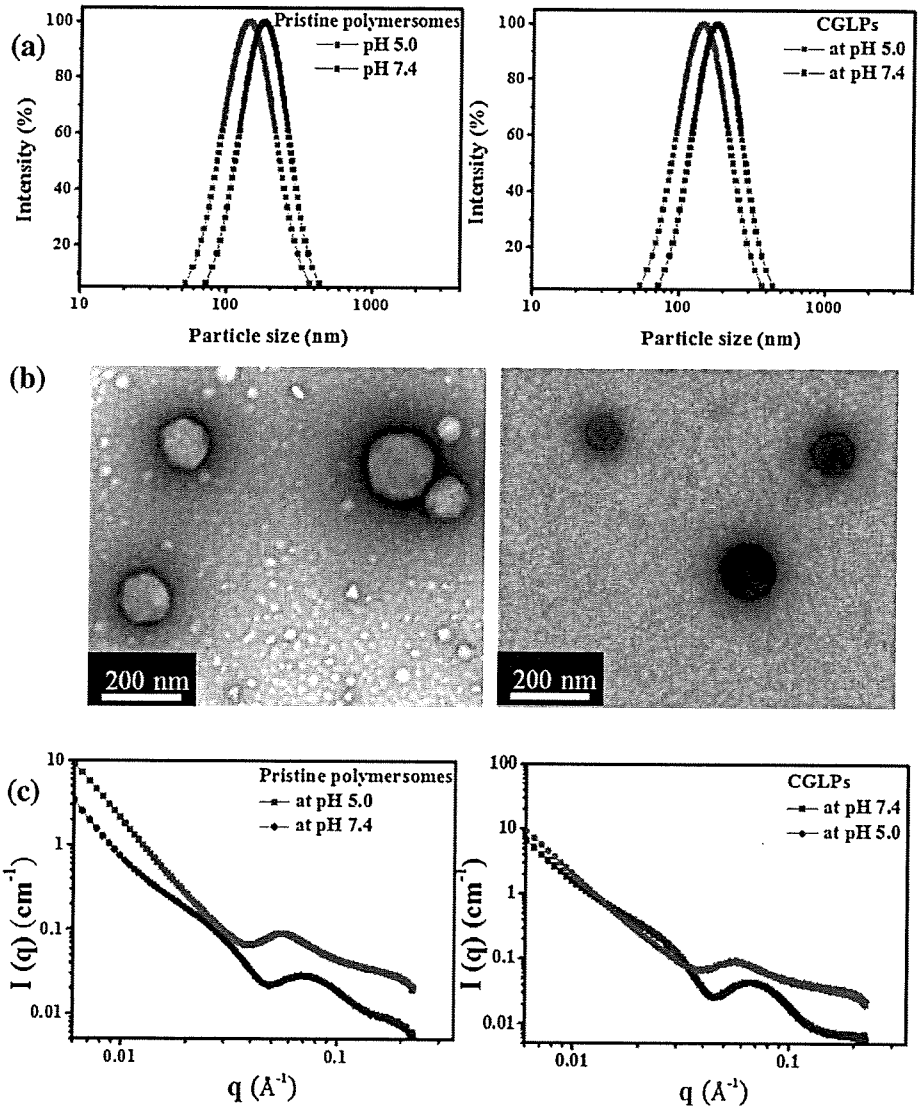

Fig. 2. Morphologic characterization of CGLPs. (a) DLS colloidal size distribution profiles, (b) TEM images and (c) SAXS profiles of pristine polymersomes (left) and CGLPs (right). The DLS and SAXS measurements were performed with particle suspensions in the pH 5.0 and 7.4 buffers, respectively. TEM sample was prepared from the nanoparticle formulations suspended in the pH 5.0 buffer solution.

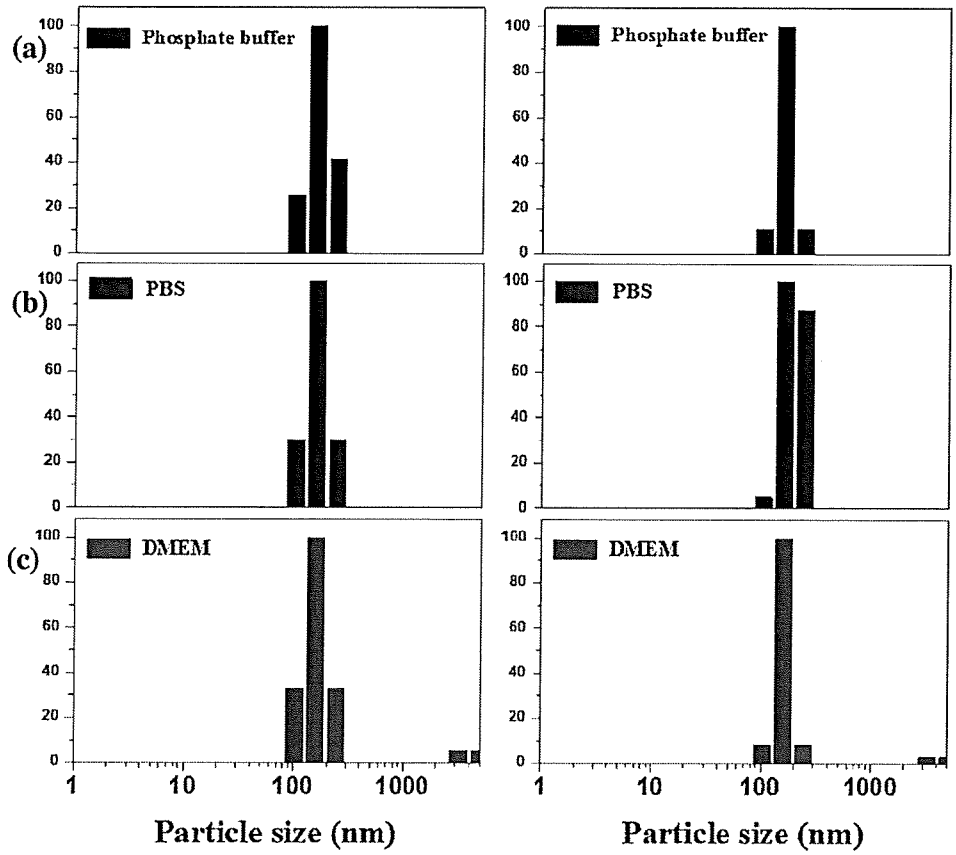

Fig. 3. DLS particle size distribution profiles of the CGLPs in (a) phosphate buffer (pH 7.4) with 200-fold dilution, in (b) PBS (0.15 M NaCl) and in (c) DMEM (10% FBS) at 37 °C for (left) 0 and (right) 72 h, respectively.

washed twice with PBS. The cells were then replaced with a fresh RPMI medium containing 10 vol% of AlamarBlue in each well. After 2 h incubation, the media/AlamarBlue solution was analyzed with optical absorbance at 570 and 600 nm and the cell viability determined by comparing the absorbance of the sample to the blank control [16]. For laser scanning confocal microscopy (LSCM) studies, HeLa cells (2×10^5 cells) seeded onto 22 mm round glass coverslips were placed in a 6-well plate and cultured overnight. The cells were then incubated with free Cy5.5 and CGLPs, respectively, at a Cy5.5 concentration of 20 μg/mL for 4 h. Cells were subsequently washed with PBS, fixed with 4% formaldehyde, and stained with Hoechst 33258 for 10 min. Cellular uptake of Cy5.5 was visualized at the excitation wavelength of 633 and emission range of 640–760 nm, respectively, with a ZESS LSM 510 META.

2.7. *In vitro imaging*

In vitro MR imaging was conducted on a 4.7 T scanner (Bruker BioSpec, 47/40 USR, Bruker Biospin, MA, USA). The T_1-weighted gradient echo phantom images of Magnevist and CGLPs of varying Gd(III) concentrations were acquired with the following parameters: TR = 200, 220, 240, 260, 280, 300, 320, 400, 500, 600, 700, 900, 1000, 1500, 2000, 3000, 5000, 8000 ms; TE = 8 ms; field of view (FOV) = 6.0 cm × 6.0 cm; flip angle of 30°; Image matrix = 256 × 256; number of signal averages = 3; Slices = 6; thickness = 1.0 mm.

In vitro NIR images of cellular uptake were obtained using an *in vivo* imaging system (IVIS, Xenogen, USA). HeLa cells (2×10^5 cells/well) in a 6-well plate were treated with CGLPs in the concentration range 0–250 μg/mL at 37 °C. After being washed twice with PBS, cells were detached with the trypsin-EDTA solution and then dispersed in 200 μL DMEM. The cellular uptake of CGLPs was then visualized at the excitation and emission wavelengths of 675 and 720 nm, respectively, with the IVIS. The blank control in the absence of HeLa cells was used for comparison.

2.8. *In vivo imaging studies*

In vivo MR imaging was performed on C57BL/6 male mice, aged 6–8 weeks. The CGLPs were injected at a Gd dose of 0.02 mmol/kg into mouse-tail vein. The standard Gd dose of Magnevist, 0.1 mmol/kg, was used for comparison. The MRI experiments were performed on a scanner using a 60-mm gradient insert and a volume resonator with 35 mm inner diameter. Animal was anesthetized with isoflurane and then placed prone with the head first in the MRI scanner. Pre-contrast and post-contrast magnetic resonance angiography images were acquired with a heavily T_1-weighted 3D fast spoiled gradient echo protocol. Scans were performed with the following imaging parameters: repetition time (TR) = 8.0 ms; echo time (TE) = 4.5 ms; flip angle = 30°; FOV = 70 mm × 70 mm × 70 mm; Image matrix = 128 × 128 × 128; number of signal averages = 3. Maximum intensity projection images were performed and analyzed [23].

Intramuscular murine prostate Tramp-C1 tumors were produced by intramuscular inoculation of 3×10^6 viable Tramp-C1 cells into the right thighs of C57BL/6 mice. Tumors around 1.5 cm in diameter were adopted for IVIS study. The CGLPs were intravenously injected with a single dose (*ca* 50 mg/kg) in 100 μL saline. Mice were imaged by IVIS (Cy5.5 filter set λ_{ex} = 675 nm/λ_{em} = 720 nm) equipped with Living Image® 3.1 software 4 and 24 h post-injection under anesthesia by inhalation

of oxygen-isoflurane. Gray-scale photographic image and fluorescence image of each sample was analyzed and overlaid using Living Image software (Xenogen, Alameda, CA).

3. Results and discussion

3.1. Preparation and characterization of CGLPs

Pristine polymersomes were obtained from the spontaneous assembly of poly(AAc-co-DSA) in aqueous solution of pH 5.0 and characterized by a D_h of *ca* 160 nm and a narrow particle size distribution (Fig. 2a). The Cy5.5-loaded polymersomes were attained by addition of Cy5.5 during polymersome preparation. To develop a diagnostic polymersome system as a dual image contrast agent, the aqueous $GdCl_3$ solution was added into the Cy5.5-loaded polymersome suspension at pH 7.4. Loading of diagnostic payloads (Cy5.5 and Gd(III)) was achieved *via* different encapsulation mechanisms; that is the association of Cy5.5 by hydrophobic effect and the binding of Gd(III) by charge attachment. The unbound payloads were eliminated by dialysis for 3 days. The loading efficiencies of Cy5.5 and Gd(III) are 73.8 ± 3.4% and 82.9 ± 8.4% as quantitatively measured by UV/Vis spectrometer and ICP-MS, respectively. The DLS data in Fig. 2a show that the CGLPs have a D_h of *ca* 165 nm and mono-modal size distribution with a polydispersity index (PDI) of 0.18, similar to that of pristine polymersomes. This is presumably because the added Cy5.5 and Gd(III) payloads amount merely to 4 wt% of the copolymer and 1.35 mol% of AAc residues, respectively, in the recipe to prepare CGLPs. The vesicle-like morphology of CGLPs was confirmed by laser light scattering. The data are summarized in Table 1. The R_g/R_h ratios, known as a measure for morphologic assessment due to the high sensitivity to assembly topology, of pristine polymersomes and CGLPs are slightly higher than the theoretical value (1.0) for non-draining thin-layer hollow spheres, but rather distinct from either uniform solid spheres (0.774) or polymer coils (1.5–1.8) [19]. This is ascribed to the self-assembly of the copolymer into rather hydrated vesicle-like particles with thick membranes [16]. The TEM images confirm that the morphology of CGLPs is in the vesicle-like spherical structure similar to the pristine polymersomes (Fig. 2b). To gain an insight into the morphology of polymeric assemblies, SAXS was utilized for CGLP structural examination. From the scattering intensity profile of the CGLP suspension at pH 5.0 (Fig. 2c), a rather sharp Bragg peak appears at high q position (*ca* 0.05 $Å^{-1}$), indicating that the CGLPs exist in the multilamellar architecture with an interlamellar distance of *ca* 11.42 nm ($d = 2\pi/q$, where q denotes the scattering vector). With the external pH being increased to 7.4, the SAXS profile of the resulting CGLPs displays a broader scattering peak. Meanwhile, the hydrodynamic size of CGLPs also increases appreciably, from 165 at pH 5.0 to 200 nm at pH 7.4 (Fig. 2c). The broadened Bragg peak of CGLPs at pH 7.4 is primarily attributed to the pH-evolved morphological transition which has been explored in detail in our previous study [15]. The pH-induced increase of the ionization degree of AAc residues inevitably leads to water influx into AAc-rich domains and subsequent expansion of the interlayer spacing of the multilamellar structure by charge repulsion possibly

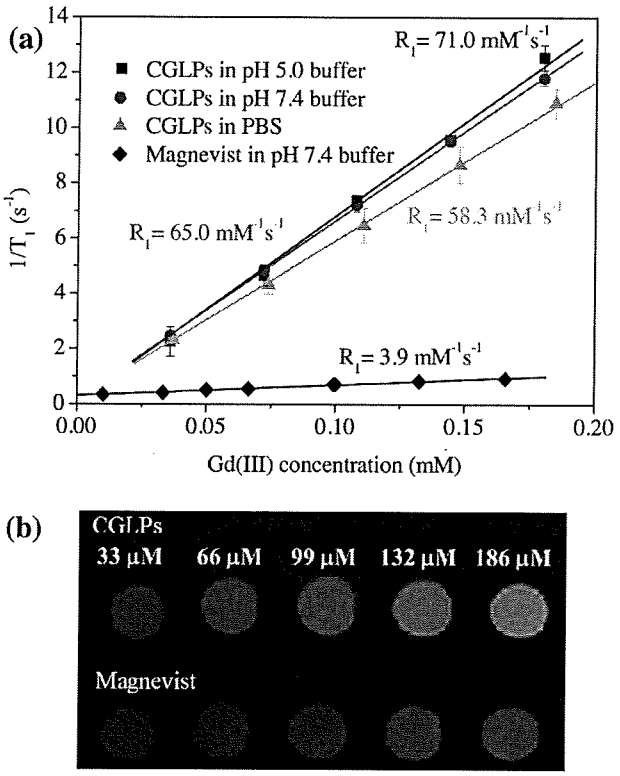

Fig. 4. (a) Relaxation rates of CGLPs in pH 7.4 phosphate buffer and PBS and of Magnevist in pH 7.4 phosphate buffer as a function of the Gd(III) concentration in the range 33–186 μM at 37 °C. (b) T_1-weighted MR images of CGLPs and Magnevist in PBS with various Gd(III) levels (TR = 600 ms/TE = 8 ms).

along with slight swelling of the multilayer structure. As a result, the primary scattering peak of CGLPs at pH 7.4 becomes broader than that at pH 5.0. Similar SAXS results were also attained for pristine polymersomes at pH 5.0 and 7.4 (Fig. 2c). The colloidal stability of CGLPs was also evaluated against the dilution effect on assembly dissociation by phosphate buffer (pH 7.4, 200-fold dilution), salt-induced aggregation in PBS, and protein adsorption-induced coagulation in DMEM (10 wt% FBS), respectively, by monitoring the hydrodynamic particle sizes at $t = 0$ and 72 h. As shown in Fig. 3, the CGLPs show an excellent *in vitro* colloidal stability not only against the dilution/salt effect but also protein adsorption in DMEM. This is primarily due to the extensive inter-polymer chain entanglement within polymer assemblies and sufficient negative charge density on the vesicular surfaces. The inter-chain entanglement prevents CGLPs from assembly dissociation by dilution. By contrast, the high-density negative surface charges of CGLPs reduce the salt/protein-induced particle coagulation by electrostatic repulsion [24].

To evaluate the loading stability of chelated Gd(III) cations under the conditions with similar physiologic temperature and ionic strength, the CGLP suspension was dialyzed against PBS at

Table 1
DLS and SLS characterizations of pristine polymersomes and CGLPs in aqueous phase.

Sample	pH	R_g^a	R_h^b	R_g/R_h	Light scattering intensity (kcps)
Pristine polymersomes	5.0	93.2 ± 7.1	78.0 ± 5.7	1.19	146.9
	7.4	118.7 ± 7.8	101.6 ± 4.1	1.17	66.9
CGLPs	5.0	98.4 ± 2.1	82.6 ± 6.2	1.19	146.1
	7.4	115.4 ± 9.1	100.2 ± 7.9	1.15	89.1

[a]Determined by SLS from scattering angle 40 to 140°, using the Berry plot analysis method.
[b]Determined by DLS at a scattering angle of 90°, using the CONTIN analysis method.

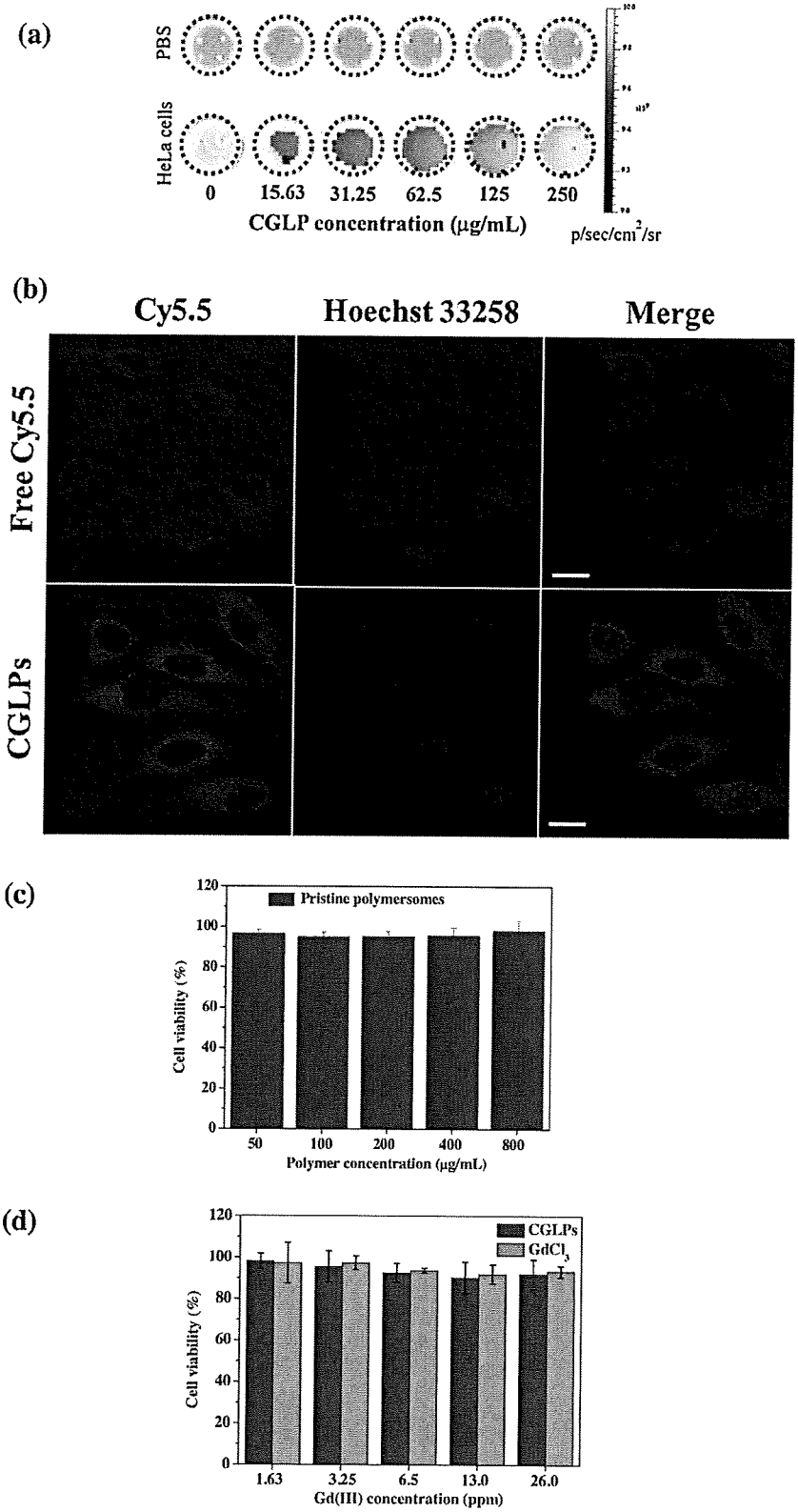

Fig. 5. (a) NIR luminescence intensity of PBS samples as a control (top) and of HeLa cells co-incubated with CGLPs of varying concentrations for 4 h (bottom). (b) LSCM images of HeLa cells incubated, respectively, with free Cy5.5 and CGLPs at 37 °C for 4 h (Cy5.5 concentration = 20 μg/mL). Cell nuclei were stained with Hoechst 33258. (c) *In vitro* cytotoxicity of pristine polymersomes and (d) of $GdCl_3$ and CGLPs against HeLa cells with respect to the blank control. Note that the variation of the Gd(III) concentration in (d) was achieved by the dilution with DMEM.

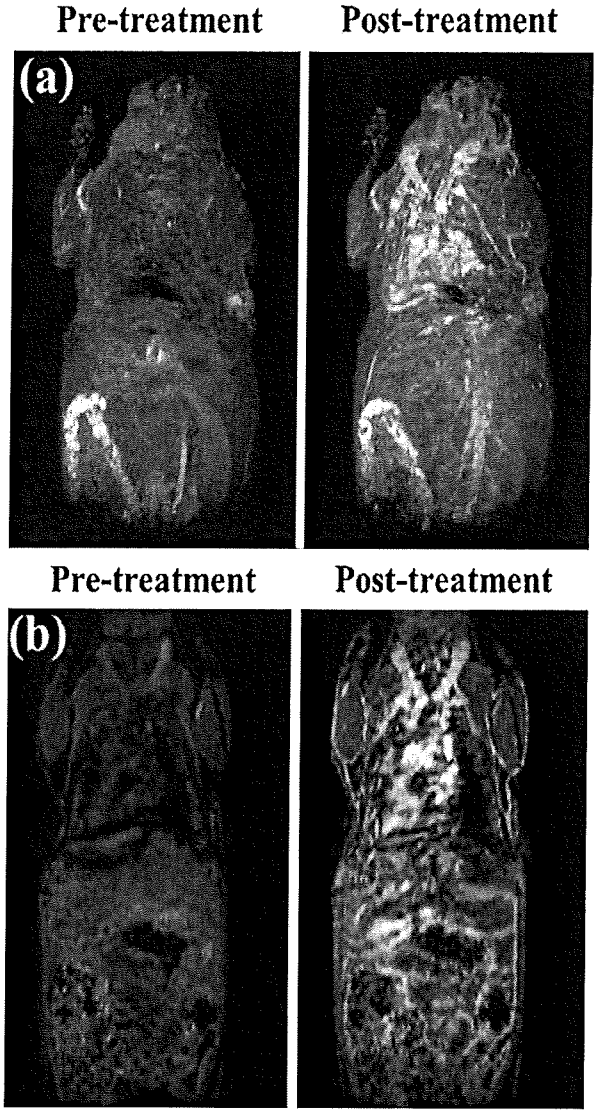

Fig. 6. MR images of C57BL/6 mice before (left) and after (right) receiving (a) CGLPs and (b) Magnevist intravenously *via* tail vein, respectively. Images were acquired prior to the injection and 5 min post-injection using a 4.7 T MRI system. The Gd dose of CGLPs administered was 5-fold lower than that of Magnevist.

37 °C for 3 days. As a result of ICP-MS measurement, the premature Gd(III) leakage of CGLPs was less than 2%, suggesting that the Gd(III) species be confined effectively within polymersomes. The cationic Gd(III) exchange with other metal ions was further examined by addition of $ZnCl_2$ or $CaCl_2$ with a concentration 5-fold higher than that of Gd(III) into the CGLP suspension and subsequent dialysis to eliminate the replaced Gd(III) cations. Based on the ICP-MS data, the Gd(III) content within CGLPs remains virtually unchanged. These results suggest that the multilamellar morphology of vesicular membranes impart the polymersomes superior metal-chelating ability to confine the entrapped Gd(III) cations inside vesicle membranes comprising ionized AAc-rich interlayers surrounding the uncharged AAc residues/lipid-bilayer islets [18]. The hydrophobic islets are rather dehydrated and closed-packed, presumably retarding the premature leakage and cationic exchange of entrapped Gd(III) cations from CGLPs.

3.2. Relaxometric measurements

The longitudinal relaxivity (r_1) of CGLP solutions was estimated by means of the inversion recovery approach in which the slope was obtained from the straight line of $1/T_1$ against Gd(III) concentration in either pH 7.4 phosphate buffer or PBS. The T_1 measurements of aqueous CGLP solutions were performed using a relaxometer at 20 MHz (0.47 T) and 37 °C. Fig. 4a shows that both the longitudinal relaxivity values of CGLP suspensions in two different media (65.0 mM^{-1} s^{-1} in pH 7.4 buffer and 58.0 mM^{-1} s^{-1} in PBS) are at least 15-fold higher than that (3.9 mM^{-1} s^{-1}) of the commercial product, Magnevist. The longitudinal relaxivity of Gd(III)-containing aqueous solution is virtually governed by several factors, including (1) the number of coordinated fast-exchanging inner sphere water molecules on Gd(III) surface, (2) the rotational correlation time of Gd(III) and (3) water exchange from Gd(III) to the bulk aqueous phase [25,26]. Comparing with Magnevist, the dramatic enhancement of the sensitivity in longitudinal relaxation times (T_1) to the concentration of Gd(III) within CGLPs can be ascribed to the entrapment of Gd(III) species within a highly hydrated vesicle membrane. This not only prolongs rotational correlation time of Gd(III) cations, but also concomitantly retains high-level water exchange from Gd(III) cations to the bulk solution. The relaxivity was slightly decreased from 65.0 mM^{-1} s^{-1} in pH 7.4 phosphate buffer (I 0.01 M) to 58 mM^{-1} s^{-1} in PBS. This is mainly due to the electrostatic screening at high salt concentration (in PBS), leading to partial reduction in water exchange rate of polymersome membrane with bulk aqueous phase [27]. With the phosphate buffer pH being adjusted to 5.0, the r_1 of CGLP suspension (71.0 mM^{-1} s^{-1}) is rather close to that (65 mM^{-1} s^{-1}) at pH 7.4, signifying that the water species can freely penetrate across the membranes even at mild acidic pH. The membrane permeability to polar solutes is virtually governed by the supramolecular packing density of polymersome membrane. With the membrane being hydrated and swollen, the membrane packing density was decreased and permeability was thus enhanced. Our previous study has shown that there are two factors governing the molecular packing inside the polymersome membrane [15]. One is the DSA content of the copolymer used to prepare polymersomes and the other is the pH of the polymersome suspension, which manipulates the ionization extent of AAc residues within polymersome membrane. Since the CGLPs were attained from the copolymer with a relatively low DSA content (*ca* 10 mol%), the molecular packing density remained low irrespective of the medium pH (either 7.4 or 5.0) while the membrane structure was additionally stabilized (particularly at pH 7.4) by extensive chelation and immobilization of Gd(III) with the ionized AAc residues. The CGLPs thus exhibited rather high longitudinal relaxivities in aqueous solution at both pH 7.4 and 5.0 as a result of the superior water permeability of the polymersome membrane. As shown in Fig. 4b, the T_1-weighted imaging contrast of CGLPs in PBS was increased proportionally with the increase of the Gd(III) concentration as conducted on a 4.7 T Biospec MRI system. In addition, the ratio of the transverse to longitudinal relaxivities (r_2/r_1 = 1.15) obtained also by MR scanner falls into the range 1.0–2.0, thereby confirming the advantageous preference of CGLPs to serve as a T_1-weighted contrast agent [28]. Being consistent with the relaxometric data, the CGLP system shows a more appreciable contrast enhancement in T_1-weighted image than Magnevist at equivalent Gd(III) levels, manifesting the ability of CGLPs to largely improve the contrast in MRI.

To evaluate the mean longitudinal relaxivity of individual CGLPs, the weight-average molar mass of CGLPs was estimated to be 1.68×10^9 g/mol by the static laser light scattering from the Berry treatment for the data analysis. Assuming that the lipid/polymeric adducts added in feed were all involved in CGLP preparation, the average number of entrapped Gd(III) species per colloidal

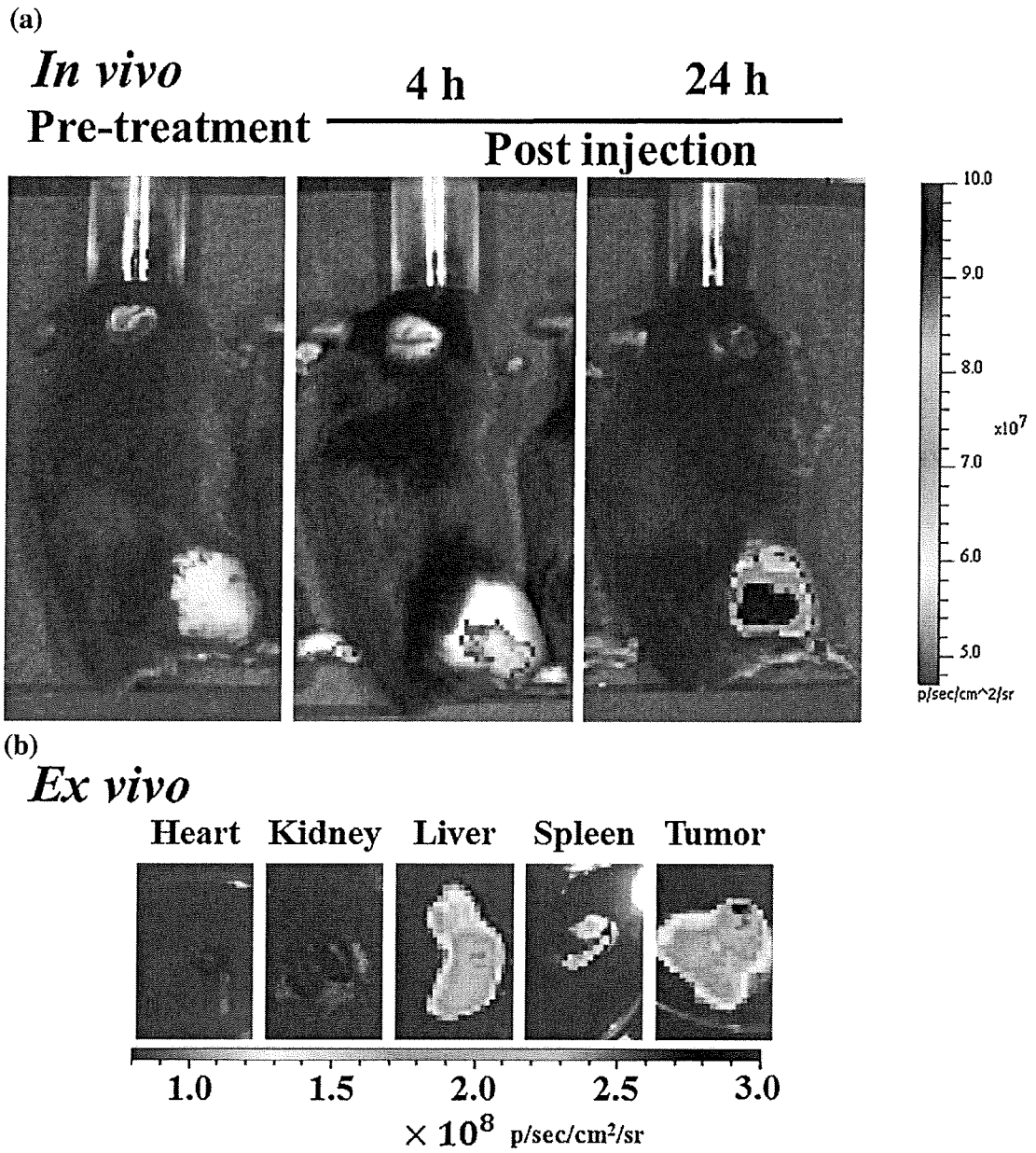

Fig. 7. (a) *In vivo* NIR fluorescence images of tumor-bearing (Tramp-C1) mice (C57BL/6) acquired after intravenous injection of CGLPs *via* tail vein. (b) *Ex vivo* fluorescence images of major organs and tumor collected from the mouse 24 h post-injection of CGLPs.

particle was estimated, according to the data of ICP-MS, to be *ca* 1.60×10^6, which gives the longitudinal relaxivity per particle *ca* $1.12 \times 10^8\ mM^{-1}\ s^{-1}$. Given as an example, this value is 300-fold higher compared to a reported Gd(III)-based polymer colloidal system (*ca* $3.2 \times 10^5\ mM^{-1}\ s^{-1}$ per colloidal particle), which exhibited a longitudinal relaxivity of $7.2\ mM^{-1}\ s^{-1}$ per Gd(III) cation with each particle containing 4.4×10^4 Gd(III) species [6]. In addition, the CGLPs demonstrate a *ca* 10^7-fold enlargement in relaxivity per system as compared to those of commercial products such as Magnevist, Omniscan, and Dotarem. These results imply a significant reduction in the Gd(III) dose required from CGLPs for MR imaging.

3.3. *In vitro endocytic uptake and cytotoxicity*

For CGLPs to act as an effective MR/NIR imaging delivery system, they should provide a significant contrast enhancement even though they are cellularly internalized. The *in vitro* cellular uptake of CGLPs by HeLa cells presumably *via* endocytosis and the resulting intracellular fluorescence intensity was examined using IVIS and LSCM, respectively. As shown in Fig. 5a for the IVIS examination, the NIR fluorescence signal of HeLa cells incubated with CGLPs increased in a proportional manner with the increase of the CGLP dose, suggesting that the CGLPs after being engulfed by HeLa cells can act effectively as an intracellular fluorescence probe. By contrast, in the absence of HeLa cells, no signal was observed in NIR image from these blank samples. In Fig. 5b, the LSCM images also clearly demonstrate that HeLa cells co-incubated with CGLPs show a much stronger intracellular Cy5.5 fluorescence signals than those with free Cy5.5. This is primarily attributed to the severe aggregation behavior of free Cy5.5 in aqueous phase by its hydrophobic nature in contrast to the well aqueous dispersion of CGLPs even in DMEM (containing 10 wt% FBS). All these results demonstrate the potential of CGLPs as an intracellular imaging system.

Nevertheless, there are two prerequisites for developing a successful delivery system of diagnostics and/or therapeutics. This includes the construction of delivery carriers, particularly for imaging, from non-cytotoxic materials which are concomitantly capable of uploading diagnostic and/or therapeutic components in an effective manner. The *in vitro* cytotoxicity of pristine polymersomes and CGLPs against HeLa cells was evaluated by the AlamarBlue assay. With being co-incubated with HeLa cells, pristine polymersomes were found quite benign towards the cells (Fig. 5c). Similarly, as shown in Fig. 5d, the cells remain rather high survival rates while in contact with either $GdCl_3$ or CGLPs in the Gd(III) concentration range employed, further implying the essential non-cytotoxic nature of CGLPs.

3.4. *In vivo* imaging study

Owing to the benign effect of CGLPs on cell survival, CGLPs were injected *via* tail vein into C57BL/6 mice for the *in vivo* biodistribution study. Magnevist was also given separately for the comparison purpose. As shown in Fig. 6a, prior to the mice receiving diagnostic agent, no appreciable change in the contrast density was observed by MRI system. By contrast, the major blood vessels and cardiac outline became all contrast-enhanced and clearly visible 5 min post injection with either a standard dose of Magnevist (0.1 mmol Gd/kg) or a 5-fold-lower Gd dose of CGLPs (0.02 mmol Gd/kg) (Fig. 6b). With the mice receiving CGLPs at a Gd dose 5-fold lower, the signal-to-noise ratio (SNR) was *ca* 179% similar to that treated with Magnevist (184%), demonstrating the potential of CGLPs in MR imaging delivery by a substantial reduction in the Gd dose. This undoubtedly minimizes the frequently encountered side effects of nephrotoxicity due to the less Gd dose being needed.

We have further investigated the *in vivo* biodistribution of CGLPs using the Tramp-C1 tumor-bearing mice (C57BL/6). As shown in Fig. 7a, at 4 and 24 h post-tail-vein-injection with CGLPs, the tumor shows a much higher Cy5.5 fluorescence signal compared to that without the CGLP treatment. This implies the passive accumulation of CGLPs for imaging delivery toward tumor operated most likely by the well-known enhanced permeability and retention effects of solid malignant neoplasm. The *ex vivo* images of tumor and major organs harvested from tumor-bearing mice 24 h post injection provide the solid evidence of the significant accumulation of CGLPs within tumor as well as spleen and liver, the major organs with high activity of reticuloendothelial system (RES) (Fig. 7b) [29]. In spite of the absence of surface PEGylation, the CGLPs show more effective accumulation within tumor as compared to diagnostic nanodevices composed mainly of gold nanostructure [30]. This is primarily attributed to sufficient negative charges on CGLP surface, which plays a crucial role in reducing protein adsorption [24] (Fig. 3) and macrophage uptake in liver and/or spleen. Comparing with other supramolecular Gd(III) complexes which required much more complicated synthesis procedures [31,32], the relatively simple preparation and diagnostics loading processes render the CGLPs themselves rather potential in diagnostic applications. In addition, the dilemma of CGLP biodistribution can be circumvented somewhat by means of, for example, delicate decoration on particle surfaces with PEG chain segments, which has been proven effective in reducing uptake of nanodevices by RES. In our previous works [17,33], polymersomes decorated on their surfaces with PEG-attached polyelectrolyte gel outlayer were developed *via* electrostatic interactions and *in-situ* covalent cross-linking. These unique functional outlayer gels can largely improve the *in vivo* colloidal stability and passive targeting to tumor site by reducing the RES uptake. Future work will concentrate on the implementation of CGLP with such functional polyelectrolyte gel outlayers for further *in vivo* study.

4. Conclusions

In this work, we have developed a novel dual-imaging diagnostic polymersome system carrying both paramagnetic Gd(III) and NIR emissive Cy5.5 for enhancing soft tissue MR and NIR image contrasts. Through the assembly of lipid-conjugated copolymer, poly(AAc-co-DSA), together with Cy5.5 in aqueous solution of pH 5.0 and the subsequent Gd(III) loading *via* charge complexation at pH 7.4, the CGLPs were attained. Cy5.5 was loaded with a satisfactory efficiency into the hydrophobic regions of polymer vesicle membranes *via* hydrophobic association. With the negative charge density, the hydration and permeability of vesicular membranes being enhanced by a pH switch from 5.0 to 7.4, the cationic Gd(III) species were easily entrapped within vesicle walls by forming extensive AAc/Gd(III) complexes. The CGLPs demonstrated a superior capability of contrast enhancement in NIR and MR imaging, particularly the *in vivo* MR and NIR image contrasts on the major blood vessels and tumor tissues. Comparing with Magnevist, the CGLPs display a similar image contrast, yet with a Gd(III) dose 5-fold lower, indicating the great potential of CGLPs as an effective imaging contrast delivery system. The *in vitro* cytotoxicity study indicated that the CGLPs are virtually non-cytotoxic. To improve the *in vivo* biodistribution, the CGLPs equipped with a folate-PEG-attached cross-linked gel outlayers on the particle surfaces for acquiring superior homing ability and biostability are now undertaking.

Acknowledgments

This work is supported by the Ministry of Science and Technology (MOST 102-2221-E-007-032-MY3 and MOST 102-2221-E-007-133-MY3) and National Tsing Hua University (103N2046E1) Taiwan. The authors also thank the National Synchrotron Radiation Research Center (Hsinchu, Taiwan) for the use of SAXS (23A1).

Appendix A. Supplementary data

Supplementary data associated with this article can be found, in the online version, at http://dx.doi.org/10.1016/j.colsurfb.2015.02.008.

References

[1] C.T. Adkins, J.N. Dobish, C.S. Brown, B. Mayrsohn, S.K. Hamilton, F. Udoji, K. Radford, T.E. Yankeelov, J.C. Gore, E. Harth, Polym. Chem. 3 (2012) 390.
[2] E.J. Werner, A. Datta, C.J. Jocher, K.N. Raymond, Angew. Chem. Int. Ed. 47 (2008) 8568.
[3] A. Datta, K.N. Raymond, Acc. Chem. Res. 42 (2009) 938.
[4] R.B. Lauffer, Chem. Rev. 87 (1987) 901.
[5] S.Q. Wang, P. Hashemi, Semin. Cutan. Med. Surg. 29 (2010) 174.
[6] Z.L. Cheng, A. Tsourkas, Langmuir 24 (2008) 8169.
[7] B.A. Moffat, T.L. Chenevert, T.S. Lawrence, C.R. Meyer, T.D. Johnson, Q. Dong, C. Tsien, S. Mukherji, D.J. Quint, S.S. Gebarski, P.L. Robertson, L.R. Junck, A. Rehemtulla, B.D. Ross, Proc. Natl. Acad. Sci. U.S.A. 102 (2005) 5524.
[8] S. Serres, M.S. Soto, A. Hamilton, M.A. McAteer, W.S. Carbonell, M.D. Robson, O. Ansorge, A. Khrapitchev, C. Bristow, L. Balathasan, T. Weissensteiner, D.C. Anthony, R.P. Choudhury, R.J. Muschel, N.R. Sibson, Proc. Natl. Acad. Sci. U.S.A. 109 (2012) 6674.
[9] K. Ghaghada, C. Hawley, K. Kawaji, A. Annapragada, S. Mukundan Jr., Acad. Radiol. 15 (2008) 1259.
[10] Z.L. Cheng, D.L.J. Thorek, A. Tsourkas, Adv. Funct. Mater. 19 (2009) 3753.
[11] W.L. Zhang, N. Li, J. Huang, S.F. Luo, M.X. Fan, S.Y. Liu, B. Muir, J.H. Yu, J. Appl. Polym. Sci. 121 (2011) 3175.
[12] T. Mizuno, K. Mohri, S. Nasu, K. Danjo, H. Okamoto, J. Control. Release 134 (2009) 149.
[13] P. Puech, D. Huglo, G. Petyt, L. Lemaitre, A. Villers, Curr. Opin. Urol. 19 (2009) 168.
[14] A.S. Wadajkar, T. Kadapure, Y. Zhang, W.N. Cui, K.T. Nguyen, J. Yang, Adv. Healthc. Mater. 1 (2012) 450.
[15] W.C. Huang, W.H. Chiang, S.J. Lin, Y.J. Lan, H.L. Chen, C.S. Chern, H.C. Chiu, Adv. Funct. Mater. 22 (2012) 2267.

[16] W.C. Huang, W.H. Chiang, Y.F. Huang, S.C. Lin, Z.F. Shih, C.S. Chern, C.S. Chiang, H.C. Chiu, J. Drug Target. 19 (2011) 944.
[17] W.H. Chiang, W.C. Huang, C.W. Chang, M.Y. Shen, Z.F. Shih, Y.F. Huang, S.C. Lin, H.C. Chiu, J. Control. Release 168 (2013) 280.
[18] H.C. Chiu, Y.W. Lin, Y.F. Huang, C.K. Chuang, C.S. Chern, Angew. Chem. Int. Ed. 47 (2008) 1875.
[19] W. Schärtl, Springer, Berlin/New York, 2007.
[20] E.K. Penott-Chang, M. Ruppel, D.V. Pergushov, A.B. Zezin, A.H.E. Muller, Polymer 52 (2011) 4296.
[21] W.H. Chiang, W.C. Huang, M.Y. Shen, C.H. Wang, Y.F. Huang, S.C. Lin, C.S. Chern, H.C. Chiu, PLoS ONE 9 (2014) e92268.
[22] G.H. Liang, L.L. Cao, H. Chen, Z.Y. Zhang, S. Zhang, S.N. Yu, X.R. Shen, J.L. Kong, J. Mater. Chem. B 1 (2013) 629.
[23] K.B. Ghaghada, M. Ravoori, D. Sabapathy, J. Bankson, V. Kundra, A. Annapragada, PLoS ONE 4 (2009) e7628.
[24] S. Patil, A. Sandberg, E. Heckert, W. Self, S. Seal, Biomaterials 28 (2007) 4600.
[25] E. Toth, L. Helm, A.E. Merbach, Top. Curr. Chem. 221 (2002) 61.
[26] S. Laurent, L.V. Elst, C. Thirifays, R.N. Muller, Langmuir 24 (2008) 4347.
[27] R. Georgieva, R. Dimova, G. Sukhorukov, G. Ibarz, H. Mohwald, J. Mater. Chem. 15 (2005) 4301.
[28] R. Hao, J. Yu, Z. Ge, L. Zhao, F. Sheng, L. Xu, G. Li, Y. Hou, Nanoscale 5 (2013) 11954.
[29] G.G. Bural, D.A. Torigian, W.G. Chen, M. Houseni, S. Basu, A. Alavi, Hell. J. Nucl. Med. 13 (2010) 23.
[30] A. Srivatsan, S.V. Jenkins, M. Jeon, Z. Wu, C. Kim, J. Chen, R.K. Pandey, Theranostics 4 (2014) 163.
[31] C.M. Andolina, P.J. Klemm, W.C. Floyd, J.M.J. Fréchet, K.N. Raymond, Macromolecules 45 (2012) 8982.
[32] M.Q. Tan, Z. Ye, D. Lindner, S.M. Brady-Kalnay, Z.R. Lu, Pharmaceut. Res. 31 (2014) 1469.
[33] Y.F. Huang, W.H. Chiang, W.C. Huang, H.H. Chen, M.Y. Shen, S.C. Lin, C.S. Chern, H.C. Chiu, J. Mater. Chem. B 2 (2014) 4988.